International Journal of Heat and Fluid Flow xxx (2009) xxx–xxx

Contents lists available at ScienceDirect

International Journal of Heat and Fluid Flow

journal homepage: www.elsevier.com/locate/ijhff

DNS of a spatially developing turbulent boundary layer with passive scalar transport

Qiang Li *, Philipp Schlatter, Luca Brandt, Dan S. Henningson

Linné Flow Centre, KTH Mechanics, Osquars Backe 18, SE-100 44 Stockholm, Sweden

ARTICLE INFO

Article history:
Received 7 November 2008
Received in revised form 12 May 2009
Accepted 29 June 2009
Available online xxxx

Keywords:
Turbulent boundary layer
Passive scalar
Direct numerical simulation (DNS)
Prandtl number

ABSTRACT

A direct numerical simulation (DNS) of a spatially developing turbulent boundary layer over a flat plate under zero pressure gradient (ZPG) has been carried out. The evolution of several passive scalars with both isoscalar and isoflux wall boundary condition are computed during the simulation. The Navier–Stokes equations as well as the scalar transport equation are solved using a fully spectral method. The highest Reynolds number based on the free-stream velocity U_∞ and momentum thickness θ is $Re_\theta = 830$, and the molecular Prandtl numbers are 0.2, 0.71 and 2. To the authors' knowledge, this Reynolds number is to date the highest with such a variety of scalars. A large number of turbulence statistics for both flow and scalar fields are obtained and compared when possible to existing experimental and numerical simulations at comparable Reynolds number. The main focus of the present paper is on the statistical behaviour of the scalars in the outer region of the boundary layer, distinctly different from the channel-flow simulations. Agreements as well as discrepancies are discussed while the influence of the molecular Prandtl number and wall boundary conditions is also highlighted. A *Pr* scaling for various quantities is proposed in outer scalings. In addition, spanwise two-point correlation and instantaneous fields are employed to investigate the near-wall streak spacing and the coherence between the velocity and the scalar fields. Probability density functions (PDF) and joint probability density functions (JPDF) are shown to identify the intermittency both near the wall and in the outer region of the boundary layer. The present simulation data will be available online for the research community.

© 2009 Elsevier Inc. All rights reserved.

1. Introduction

The understanding of the spreading of a passive scalar in turbulent flows was initially gained solely through wind tunnel experiments. The early studies of heat transfer were performed by e.g. Corrsin (1952) and Warhaft and Lumley (1978) in grid-generated turbulence and homogeneous turbulence. Hishida and Nagano (1979) and Nagano and Tagawa (1988) measured various types of moments of velocity and scalar fluctuations in fully developed pipe flow to investigate the transport mechanism in turbulence and to correlate the transfer processes of momentum and scalar with coherent motions. In particular, the importance of the coherent motions in the turbulent diffusion process of Reynolds-stress components and scalar fluxes was demonstrated for the first time. Later, Mosyak et al. (2001) and Hetsroni et al. (2001) carried out experiments to study the wall-temperature fluctuations under different wall-boundary conditions and the thermal coherent structure in a fully developed channel flow. For turbulent boundary-layer flows, Perry and Hoffmann (1976) examined the similarity between the Reynolds shear stress $\langle u'v' \rangle$ and scalar flux $\langle v'\theta' \rangle$ using quadrant analysis. However, the Reynolds-stress $\langle u'v' \rangle$ was analysed in the (u, v) plane and the turbulent scalar flux $\langle v'\theta' \rangle$ in the (v, θ) plane. Therefore the correspondence between fluids motions and scalar transport was not strictly specified. Subramanian and Antonia (1981) measured several quantities in a slightly heated boundary layer to address the effect of Reynolds number. Krishnamoorthy and Antonia (1987) and Antonia et al. (1988) investigated the temperature dissipation and the correlation between the longitudinal velocity fluctuation and temperature fluctuation in the near-wall region.

Due to the rapid progress in high-performance computers, direct numerical simulation (DNS) of turbulent flows involving passive scalars, especially in channel geometry, has matured to an important research tool during the past few decades. The first direct numerical simulations of passive scalar transport were performed by Rogers et al. (1986) in a homogeneous shear flow. Numerical simulations in channel geometry were pioneered by Kim and Moin (1989) with $Pr = 0.1$, 0.71 and 2.0 at $Re_\tau = 180$ where Re_τ is the Reynolds number based on the friction velocity u_τ and the channel half width h and Pr is the molecular Prandtl number. Heat is introduced by an internal source created and removed from both walls. A high correlation between the streamwise velocity and temperature was found in the wall region. Later, Kasagi et al. (1992) and Kasagi and Ohtsubo (1993) performed DNS at $Re_\tau = 150$ with $Pr = 0.71$ and 0.025. The

* Corresponding author. Tel.: +46 8 790 68 76.
E-mail address: qiang@mech.kth.se (Q. Li).

0142-727X/$ - see front matter © 2009 Elsevier Inc. All rights reserved.
doi:10.1016/j.ijheatfluidflow.2009.06.007

Please cite this article in press as: Li, Q., et al. DNS of a spatially developing turbulent boundary layer with passive scalar transport. Int. J. Heat Fluid Flow (2009), doi:10.1016/j.ijheatfluidflow.2009.06.007

Nomenclature

c_p	specific scalar capacity
h	channel half width
H_{12}	shape factor
k	scalar conductivity
p	pressure
Pe	Péclet number = $Re\ Pr$
Pr	molecular Prandtl number or Schmidt number = $\frac{\nu}{\alpha}$
Pr_t	turbulent Prandtl number
q_w	rate of the scalar transfer from the wall to the flow = $-k\frac{\partial\theta}{\partial y}\|_{y=0}$
Re	Reynolds number
$Re_{\delta_0^*}$	Reynolds number based on the inlet displacement thickness δ_0^*
Re_θ	Reynolds number based on the momentum thickness θ
Re_τ	Reynolds number based on the friction velocity u_τ
St	Stanton number = $\frac{q_w}{\rho U_\infty c_p(\theta_w-\theta_\infty)}$
t	time
u_i, u, v, w	instantaneous velocity components in the streamwise, wall-normal and spanwise direction (in direction i)
u_τ	friction velocity = $\sqrt{\frac{\tau_w}{\rho}}$
U_∞	free-stream mean velocity
x_i, x, y, z	Cartesian coordinates in the streamwise, wall-normal and spanwise direction (in direction i)
y_L	height of the domain
$\mathcal{O}$	Landau symbol (order of)
$\mathscr{P}$	production of turbulent energy
$\mathscr{U}_i$	Blasius laminar base flow

subscript

f	properties of the fluid
w	properties at the wall
∞	properties in the free-stream
rms	root-mean-square value of the quantity

superscript

$\hat{}$	dimensional term for the variable quantity
$'$	fluctuating part
$+$	scaling in viscous (wall) units
out	scaling in outer units
$\langle\rangle$	average over time and the homogeneous direction

Greek symbols

α	scalar diffusivity = $\frac{k}{\rho c_p}$
α_t	eddy diffusivity = $-\frac{\langle v'\theta'\rangle}{\frac{\partial\langle\theta\rangle}{\partial y}}$
β	pressure gradient coefficient = $\frac{\delta^*}{\tau_w}\frac{dp}{dx}\|_{free-stream}$
δ^*	displacement thickness
δ_0^*	inlet displacement thickness
δ_θ^{99}	99% local scalar boundary-layer thickness
ε	dissipation of turbulent energy
Ξ	log-law diagnostic function
Ξ_θ	log-law diagnostic function for scalar
θ	momentum thickness
θ	scalar
θ_i	scalar i
θ_τ	friction scalar = $\frac{q_w}{\rho c_p u_\tau}$
θ_w	scalar concentration at the wall
θ_∞	scalar concentration in the free stream
κ	von Kármán constant
κ_θ	von Kármán constant for the scalar
λ	fringe function
λ	streak spacing
ν	kinematic viscosity = $\frac{\mu}{\rho}$
ν_t	turbulent eddy viscosity = $-\frac{\langle u'v'\rangle}{\frac{\partial\langle u\rangle}{\partial y}}$
ρ	density
τ_w	shear stress at the wall

scalar-fluxes budgets were shown and the low Pr number effects were discussed. However, the Reynolds number of these simulations still remains at a low value. Wikström (1998) performed a DNS at a higher Reynolds number of $Re_\tau = 265$ with $Pr = 0.71$. Abe et al. (2004) reached up to $Re_\tau = 1020$ and $Pr = 0.025$ and 0.71. All these simulations are done, however, with a Prandtl number lower than two. This is due to the fact that the smallest scales in the scalar fluctuation decrease with the increase of Pr. Therefore the DNS becomes an even more difficult task when the Prandtl number is high. With the help of larger parallel computers, Kawamura et al. (1998) performed the DNS in periodic channel flow at $Re_\tau = 180$ but for a wider range of Pr from 0.025 to 5.0. Later, Tiselj et al. (2001) performed a channel DNS at $Re_\tau = 150$ with Pr from 0.71 to 7. In his work, the ideal isoflux boundary condition was compared to the previous results and underestimated values for the wall-temperature fluctuations of the previous simulations were reported. Recently, Redjem-Saad et al. (2007) performed a DNS in a fully turbulent pipe flow to explore the impact of the wall curvature on the turbulent heat transfer. The Reynolds number based on the pipe radius is 5500 ($Re_\tau = 186$) and the Pr varies from 0.026 to 1. For pipe flows, slightly more intense temperature fluctuations than in channel flow were found.

However, for flat-plate boundary layers with zero pressure gradient (ZPG), which is a relevant canonical flow case for theoretical, numerical as well as experimental studies, relatively few numerical results have been published for medium or high Reynolds numbers. The direct numerical simulation by Spalart (1988) using an innovative spatio-temporal approach provided valuable data at $Re_\theta = 300,\ 670,\ 1410$. Later, Komminaho and Skote (2002) performed a true spatial DNS up to $Re_\theta = 700$. Concerning boundary-layer simulations with passive scalars, to our knowledge the first DNS was performed by Bell and Ferziger (1993) up to a medium Reynolds number of $Re_\theta = 700$ with Pr being 0.1, 0.71 and 2.0. Later, a DNS was performed by Kong et al. (2000) up to a lower Reynolds number of $Re_\theta = 420$ and $Pr = 0.71$ with isothermal and isoflux boundary conditions. Recently, Hattori et al. (2007) performed a DNS to study the buoyancy effects on the boundary layer starting from Reynolds number of $Re_\theta = 1000$ to $Re_\theta = 1200$ and $Pr = 0.71$. A new DNS was performed by Tohdoh et al. (2008) up to a low Reynolds number of $Re_\theta = 420$, with $Pr = 0.71$ and 2.0.

This paper is a study of passive scalar transport in a turbulent boundary layer spatially developing over a flat plate with zero pressure gradient (ZPG). The investigation is performed using direct numerical simulation (DNS). A spatial formulation (inflow/outflow setting) was adopted since it is the best model for a boundary layer which grows in the downstream direction rather than in time. Moreover, all the scalars were simulated simultaneously, i.e. one velocity field accommodates all the scalars. The Reynolds number $Re_{\delta_0^*}$ based on the free-stream velocity U_∞ and the inlet displacement thickness δ_0^* is 450 and Prandtl number Pr are chosen to be 0.2, 0.71 and 2.0. Isoscalar and isoflux wall boundary conditions are employed for comparison. Since similarities exist between the boundary layer and channel flow in the near-wall region, this study mainly focuses on the outer region of the boundary layer, i.e. the wake region. Based on the present data, the scalings based on the Prandtl number are also proposed for various

Please cite this article in press as: Li, Q., et al. DNS of a spatially developing turbulent boundary layer with passive scalar transport. Int. J. Heat Fluid Flow (2009), doi:10.1016/j.ijheatfluidflow.2009.06.007

scalar quantities and also for the budgets of the scalar fluxes in both inner and outer units. The goal of this paper is to extend our knowledge about the scalar transport in turbulent boundary-layer flows to a wider range of both Reynolds number and Prandtl numbers. In addition, a data base for the research community is generated, which can be useful in particular for modelling purposes.

2. Numerical methodology

2.1. Governing equations and numerical method

The three-dimensional, time-dependent Navier–Stokes equations for incompressible flow as well as the transport equation for the passive scalar in non-dimensional form using the summation convention are given by

$$\frac{\partial u_i}{\partial x_i} = 0, \tag{1}$$

$$\frac{\partial u_i}{\partial t} + u_j \frac{\partial u_i}{\partial x_j} = -\frac{\partial p}{\partial x_i} + \frac{1}{Re_{\delta_0^*}} \frac{\partial^2 u_i}{\partial x_j \partial x_j}, \tag{2}$$

$$\frac{\partial \theta}{\partial t} + u_i \frac{\partial \theta}{\partial x_i} = \frac{1}{Re_{\delta_0^*} Pr} \frac{\partial^2 \theta}{\partial x_i \partial x_i} = \frac{1}{Pe} \frac{\partial^2 \theta}{\partial x_i \partial x_i}, \tag{3}$$

where $(x_1, x_2, x_3) = (x, y, z)$ are the Cartesian coordinates in the streamwise, wall-normal and spanwise direction, respectively. $(u_1, u_2, u_3) = (u, v, w)$ are the corresponding instantaneous velocity components, t represents the time, p is the pressure and θ the scalar quantity. The Reynolds number $Re_{\delta_0^*}$ is based on the free-stream velocity U_∞ and the inlet displacement thickness δ_0^* while Pr denotes the molecular Prandtl (or Schmidt) number and $Pe = Re_{\delta_0^*} Pr$ for the Péclet number.

In the present paper, the dimensional variables are non-dimensionalised as in Kong et al. (2000), i.e.

$$u_i = \frac{\hat{u}_i}{U_\infty}, \quad x_i = \frac{\hat{x}_i}{\delta_0^*}, \quad p = \frac{\hat{p}}{\rho U_\infty^2}, \quad t = \frac{U_\infty \hat{t}}{\delta_0^*}, \tag{4}$$

$$\theta = \frac{\theta_w - \hat{\theta}}{\theta_w - \theta_\infty}, \quad \text{for the isoscalar boundary condition,} \tag{5}$$

$$\theta = 1 - \frac{k(\hat{\theta} - \theta_\infty)}{q_w \delta_0^*}, \quad \text{for the isoflux boundary condition.} \tag{6}$$

The dimensional reference quantities are defined as follows. U_∞ is the free-stream velocity, δ_0^* the inlet displacement thickness, ρ the density, k the scalar conductivity, q_w the scalar flux at the wall, θ_w the scalar concentration on the wall and θ_∞ the scalar concentration in the free-stream. The hat $\hat{}$ denotes the dimensional term for the variable quantities, i.e. $u_i,\ x_i,\ p,\ t$ and θ.

The simulation code (Chevalier et al., 2007) used in the present study employs a pseudo-spectral method comparable to that used by Kim et al. (1987). Fourier series expansion is used in streamwise and spanwise directions (wall-parallel directions) assuming periodic boundary conditions. In the wall-normal direction, Chebyshev expansions employing the Chebyshev-tau method are used. The time advancement uses a four-step third-order Runge-Kutta scheme for the nonlinear terms and a second-order Crank–Nicolson scheme for the linear terms. The nonlinear terms are calculated in physical space to avoid convolution sums. Aliasing errors are removed by using the 3/2-rule in the wall-parallel directions. Fig. 1 shows the computational box together with a contour plot of an instantaneous scalar fluctuation. To fulfil the periodic boundary conditions in the streamwise direction, a "fringe region" (Bertolotti et al., 1992) is added at the downstream end of the domain. It is implemented by adding a volume force F_i to the Navier–Stokes equations. The force is of the form

$$F_i = \lambda(x)(\mathscr{U}_i - u_i) \tag{7}$$

with $\mathscr{U}_i$ being the desired inflow condition. Note that the fringe forcing is also applied for the scalar field in a similar fashion. The fringe function $\lambda(x)$ which has continuous derivatives of all orders has a prescribed shape to minimise the upstream influence (Nordström et al., 1999) and is non-zero only in the fringe region. In the fringe region, the outflow is forced by the volume force to the laminar inflow condition which is a Blasius boundary-layer profile. In addition, to trigger rapid (natural) laminar-turbulent transition, a random volume forcing located at a short distance downstream of the inlet ($x = 10,\ Re_x = 72,950$) is used. The trip forcing can be used to generate noise at low amplitude or turbulence. The volume force is directed normal to the wall with a steady amplitude and a time-dependent amplitude. The generated noise has a uniform distribution covering all the frequencies lower than the cutoff frequency corresponding to $\frac{\pi}{2}$ in the present DNS. The turbulent field generated by the trip force leads to very good quality at the expense of a slightly enlarged transitional inflow region. In particular, there are no streamwise correlations in the fluctuations as opposed to e.g. the rescaling and recycling method employed by Kong et al. (2000).

2.2. Boundary condition

The velocity and scalar fields are periodic in the horizontal directions while boundary conditions at the wall and in the free-stream are needed to solve the governing equations.

At the solid wall, the no-slip boundary conditions for the velocities

$$u|_{y=0} = 0, \quad v|_{y=0} = 0, \quad w|_{y=0} = 0, \quad \left.\frac{\partial v}{\partial y}\right|_{y=0} = 0, \tag{8}$$

are applied. For the boundary conditions in the free-stream, a Neumann condition, i.e.

$$\left.\frac{\partial u_i}{\partial y}\right|_{y=y_L} = \left.\frac{\partial \mathscr{U}_i}{\partial y}\right|_{y=y_L}, \tag{9}$$

is imposed with y_L being the height of the domain and $\mathscr{U}_i(x, y)$ the Blasius laminar base flow.

In the present implementation for the scalar field, two types of wall-boundary conditions are available. Similar to those used by Kong et al. (2000), one is an isoscalar wall and the other an isoflux wall. These two kinds of wall-boundary conditions are given by

$$\theta|_{y=0} = 0 \quad \text{for the isoscalar boundary condition,} \tag{10}$$

$$\left.\frac{\partial \theta}{\partial y}\right|_{y=0} = 1 \quad \text{for the isoflux boundary condition.} \tag{11}$$

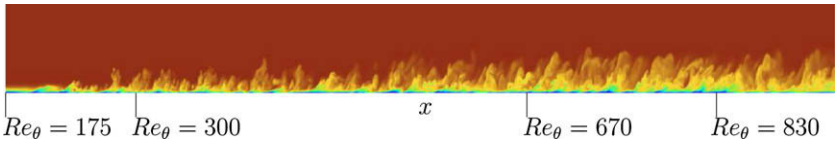

Fig. 1. Instantaneous contour plot of the fluctuating scalar field in a x–y plane, starting from $Re_\theta = 175$ to $Re_\theta = 850$. Note that the fringe region is not shown in the figure. The box height is enlarged by a factor of two.

Please cite this article in press as: Li, Q., et al. DNS of a spatially developing turbulent boundary layer with passive scalar transport. Int. J. Heat Fluid Flow (2009), doi:10.1016/j.ijheatfluidflow.2009.06.007

They corresponds to two limiting cases of the physical configuration (Tiselj et al., 2001), i.e. the scalar activity ratio being 0 for an isoscalar wall and ∞ for an isoflux wall where the scalar activity ratio is defined as $\sqrt{\rho_f c_{pf} k_f / \rho_w c_{pw} k_w}$ with ρ, c_p and k being density, scalar capacity and conductivity, respectively. The subscript f corresponds to the properties of the fluid where subscript w corresponds to the ones of the wall. For the boundary condition in the free-stream, a Dirichlet condition is imposed. A Neumann condition was also tested and the results turned out to be indistinguishable to those obtained with the Dirichlet condition. The boundary condition in the free-stream thus reads

$$\theta|_{y=y_L} = 1. \tag{12}$$

2.3. Simulation parameters

The computational box has a dimension of $750\delta_0^* \times 40\delta_0^* \times 34\delta_0^*$ in the streamwise, wall-normal and spanwise directions, respectively. The corresponding resolution is $1024 \times 289 \times 128$ which gives a grid spacing of 17, 0.025–4.6 and 6.3 (in viscous units and based on the friction velocity at the $x = 150$ or $Re_\theta = 400$) in the three directions. The Reynolds number based on the free-stream velocity U_∞ and momentum thickness θ at the inlet is $Re_\theta = 175$ and $Re_\theta = 830$ at the outlet. A comparison of the wall-normal resolution with the corresponding Kolmogorov and Batchelor scales for $Pr = 2.0$ is shown in Fig. 2. It can be concluded that a sufficient amount of grid points is used in the wall-normal direction.

A summary of the molecular Prandtl number together with the wall-boundary condition and the boundary-layer thickness, based on the 99% thickness, for all the scalars is listed in Table 1.

All results presented unless specified are averaged results. The average, denoted by the angular brackets, was performed over both time and the homogeneous spanwise direction. The corresponding fluctuating part is denoted by a prime. The averaging time after the initial transient is about 12,000 time units $\left(\frac{\delta_0^*}{U_\infty}\right)$ corresponding to $t^+ = 13,500$ in viscous units to make sure that all the statistics are sufficiently converged.

3. Results

The present paper is focused on the results pertaining to the scalar transport. In the interest of space, only one representative result of the mean velocity profile compared with other DNS data is shown, other hydrodynamic results (stresses, budgets, etc.) are not shown here. However, these hydrodynamic results were carefully validated and compared with other available numerical and experimental results and the agreements are very good in general, see Li et al. (2008).

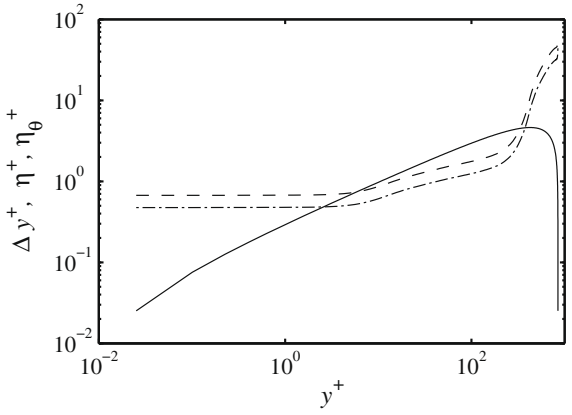

Fig. 2. Resolution check. — Wall-normal resolution Δy^+, - - - Kolmogorov scale η^+, – · – Batchelor scale η_θ^+ for $Pr = 2.0$.

3.1. Spatial evolution and flow quality

The shape factor H_{12}, defined as the ratio between the displacement thickness δ^* and the momentum thickness θ, provides a direct assessment of the flow field. As seen in Fig. 3a, a slow decrease of H_{12} with the increase of the Reynolds number in the turbulent region is observed and the agreement with the experimental data is good in the fully turbulent region close to the outlet, $Re_\theta = 830$, $H_{12} = 1.49$. The variation of the ratio of the integrated turbulent kinetic energy production $\mathscr{P}$ and dissipation ε along the streamwise direction is shown in Fig. 3b. Based on this figure, the range of Reynolds number in which the boundary layer can be assumed to be in equilibrium is for the present DNS from about $Re_\theta = 350$ to 830.

The non-dimensional parameter β related to the pressure gradient is defined as

$$\beta = \frac{\delta^*}{\tau_w} \frac{\mathrm{d}p}{\mathrm{d}x}\bigg|_{free-stream}, \tag{13}$$

where δ^* is the displacement thickness and τ_w is the shear stress at the wall. The β calculated from the simulation is of $\mathscr{O}(10^{-9})$ indicating that the flow far away from the wall is indeed subjected to zero pressure gradient.

Österlund et al. (1999) suggested a turbulent correlation for the skin-friction coefficient which reads,

$$c_f = 2\left(\frac{1}{0.384} \ln Re_\theta + 3.75\right)^{-2}. \tag{14}$$

The present results of the skin-friction coefficient compare well with this correlation even at comparably low Reynolds numbers.

The Stanton number St for a scalar boundary layer is the counterpart of the skin-friction coefficient for a momentum boundary layer. This non-dimensional scalar-transfer coefficient is defined by

$$St = \frac{q_w}{\rho U_\infty c_p (\theta_w - \theta_\infty)}, \tag{15}$$

where q_w is the rate of the scalar transfer from the wall to the flow, ρ is the density of the fluid, U_∞ is the free-stream velocity, c_p is the specific scalar, and θ_w and θ_∞ are the scalar concentrations at the wall and in the free-stream, respectively. The variations of the Stanton number with different downstream positions are shown in Fig. 4. The turbulent correlation according to Kays and Crawford (1993) which reads

$$St = 0.0125 Pr^{-\frac{2}{5}} Re_\theta^{-\frac{1}{4}}, \quad Pr > 0.5, \tag{16}$$

is included for comparison. The difference might be related to the fact that the correlations suggested by Kays and Crawford (1993) are for high Reynolds numbers. An overshoot of the peak is observed which also exists in the profile of the skin-friction coefficient, see e.g. Brandt et al. (2004). The overshoot is consistent with the general behaviour of spectral methods applied to transitional flows and it is slightly diminished with increased resolution. It is observed that the overshoot vanishes for the scalars with isoflux wall-boundary condition.

3.2. Instantaneous fields

Fig. 5 shows the instantaneous streamwise disturbance velocity at $y^+ \approx 7$ in the (x, z) plane as well as the corresponding scalar fluctuations. All the plots are obtained at the same time instant, and

Please cite this article in press as: Li, Q., et al. DNS of a spatially developing turbulent boundary layer with passive scalar transport. Int. J. Heat Fluid Flow (2009), doi:10.1016/j.ijheatfluidflow.2009.06.007

Table 1
Parameters for the scalars. Note that the boundary-layer thicknesses δ_{99}^+ are in viscous units and measured at $Re_\theta = 830$. The corresponding velocity boundary-layer thickness is about $\delta_{99}^+ = 315$ at $Re_\theta = 830$.

Scalar no.	θ_1	θ_2	θ_3	θ_4	θ_5
Wall-boundary condition	Isoscalar	Isoscalar	Isoflux	Isoscalar	Isoflux
Prandtl number Pr	0.2	0.71	0.71	2.0	2.0
Boundary-layer thickness δ_{99}^+	365	340	340	320	320

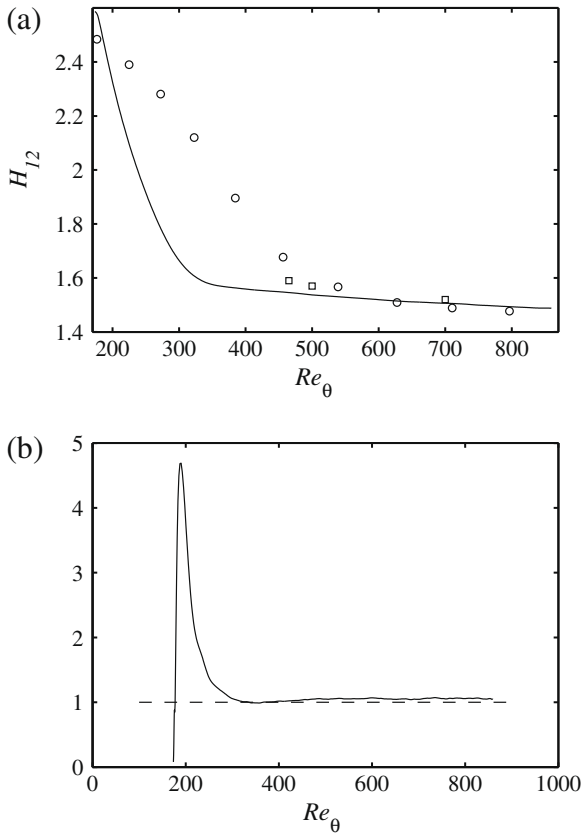

Fig. 3. Streamwise evolution of the shape factor H_{12} and the ratio of the wall-normal integrated turbulent kinetic energy production $\mathscr{P}$ and dissipation ε. — Present DNS, ∘ T3A (Roach and Brierley, 1992), □ (Purtell et al., 1981). (a) shape factor H_{12}, (b) $\frac{\int_0^\infty \mathscr{P} dy}{\int_0^\infty \varepsilon dy}$.

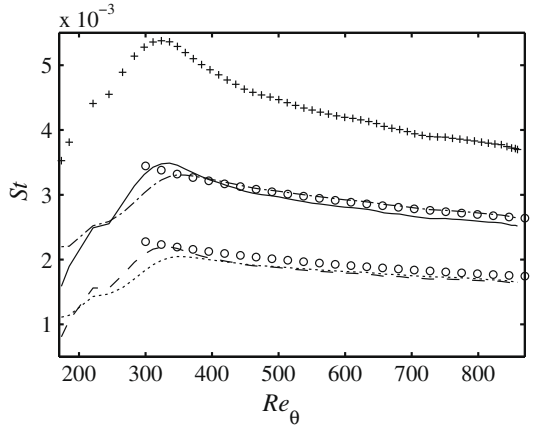

Fig. 4. Streamwise evolution of the Stanton number St. + θ_1, — θ_2, -·- θ_3, - - -θ_4, ... θ_5, ∘ (Kays and Crawford, 1993).

the visualised box is centred around $Re_\theta = 625$ and has a length of $\Delta x^+ = 2000$ and width of $\Delta z^+ = 700$ in viscous units. The viscous unit is defined by the friction velocity u_τ at the centre of the domain, i.e. $x = 350$, $Re_x = 189,500$ and $Re_\theta = 625$. Streaky structures are clearly observed and a strong similarity exists between the velocity field and the scalar field, mainly $Pr = 0.71$. The regions of low and high scalar concentrations are elongated in the streamwise direction with a mean spanwise spacing similar to that of the streamwise velocity fluctuation. Finer structures with stronger spanwise and wall-normal gradients are observed with increasing Pr. In the case of the isoflux wall-boundary condition, a clear difference can be observed: the scalar fluctuations are enhanced by the isoflux boundary condition in contrast to the ones with isoscalar boundary condition. It is also consistent with previous work by e.g. Kong et al. (2000) that the low-speed fluids are associated with low scalar concentration region and high-speed fluids with high scalar concentration region.

3.3. Mean results and turbulence intensities

For the mean profile and fluctuations of the velocity field, good agreements are observed with the DNS data from Spalart (1988) and the DNS data from Komminaho and Skote (2002) as seen in Fig. 6. A small deviation can be observed for the mean streamwise velocity profile when comparing to Spalart (1988). This is probably due to the temporal approach used for the latter simulation and is also seen in other boundary-layer simulations, e.g. Schlatter et al. (in press). The von Kármán constant κ used in the log-law is 0.41 and it gives good agreement for this comparably low Reynolds number. The log-law diagnostic function $\Xi = y^+ \frac{d<u>^+}{dy^+}$ is plotted in Fig. 7. This sensitive function Ξ is supposed to approach a constant value of the inverse von Kármán constant $\frac{1}{\kappa}$ in the overlap region according to the log-law (Nagib et al., 2007). As seen from the plot, the present DNS does not yet have a well developed logarithmic overlap region due to the comparably low Reynolds number.

The von Kármán constant for the mean scalar distributions κ_θ, is assumed to be independent of the Prandtl number and the Reynolds number in the logarithmic region. Similar to the diagnostic function for the velocity field, a constant log-law diagnostic function for scalar fields Ξ_θ, defined as $y^+ \frac{d<\theta>^+}{dy^+}$, is plotted in Fig. 8a. The present κ_θ is chosen to be 0.41 which is close to the channel-flow results by Kawamura et al. (1999) of about 0.4 but smaller than 0.47 suggested by Kader (1981).

The root-mean-square (RMS) of the fluctuations for different scalars are shown in Fig. 8b which clearly demonstrates the effects of the different boundary conditions. The data with isoscalar boundary condition go to zero as the wall is approached whereas the cases with isoflux boundary condition remain finite. Far away from the wall, the profiles of the RMS of the scalar fluctuations with different wall-boundary conditions collapse with each other indicating that the influence from the boundary conditions is only confined to the near-wall region. The limiting value of the scalar variance for θ_3 $(Pr = 0.71)$ with isoflux boundary condition was reported to be 2.0 and independent of the Reynolds number by Kong et al. (2000). However, having a higher Reynolds number range for the present DNS, a slight increase of the limiting wall value for

Please cite this article in press as: Li, Q., et al. DNS of a spatially developing turbulent boundary layer with passive scalar transport. Int. J. Heat Fluid Flow (2009), doi:10.1016/j.ijheatfluidflow.2009.06.007

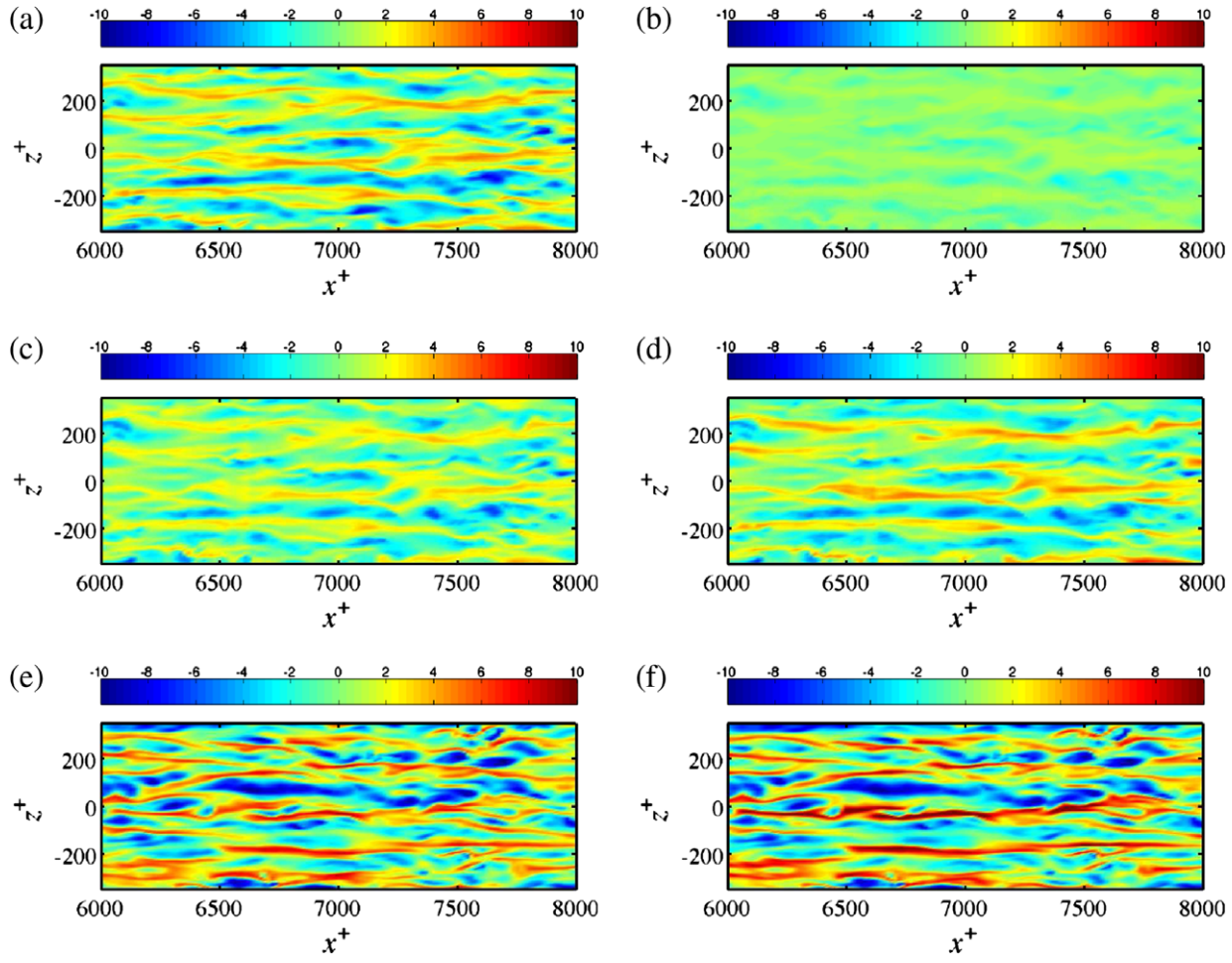

Fig. 5. Instantaneous flow and scalar fields at $y^+ \approx 7$. (a) u'^+, (b) $\theta_1'^+$, (c) $\theta_2'^+$, (d) $\theta_3'^+$, (e) $\theta_4'^+$, (f) $\theta_5'^+$.

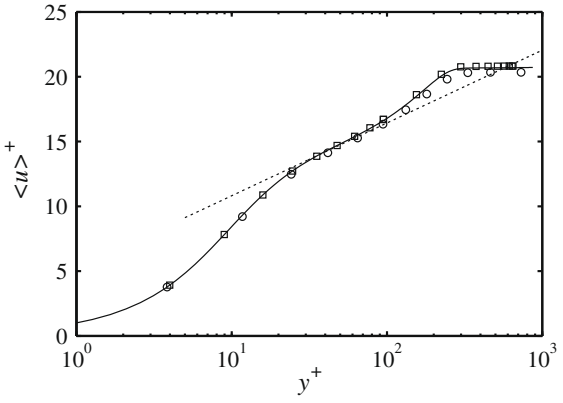

Fig. 6. Comparison of the mean streamwise velocity $\langle u \rangle^+$ with other numerical simulations. — Present DNS at $Re_\theta = 670$, ∘ (Spalart, 1988) at $Re_\theta = 670$, □ (Komminaho and Skote, 2002) at $Re_\theta = 670$, ... $\langle u \rangle^+ = \frac{1}{\kappa} \ln y^+ + 5.2$ with $\kappa = 0.41$.

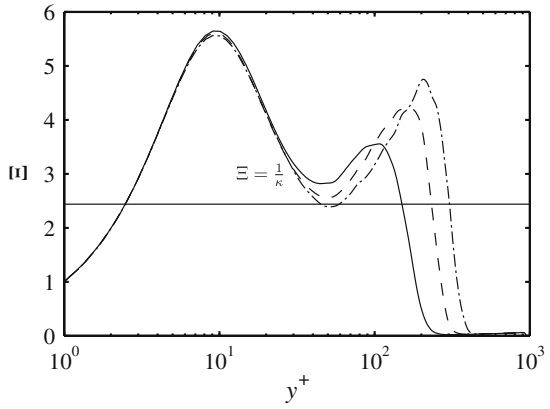

Fig. 7. Profile of the mean velocity and the diagnostic function Ξ at different Reynolds numbers. — at $Re_\theta = 390$, - - - at $Re_\theta = 620$, – · – at $Re_\theta = 830$, $\kappa = 0.41$.

increasing Reynolds number was observed for both θ_3 and θ_5, roughly following $Re_\theta^{0.1}$. For example, a value of 2.12 at $Re_\theta = 850$ was found for θ_3 ($Pr = 0.71$). However, to what extent this growth continues for high Reynolds number is still unclear due to the limited maximum Re_θ in the present study. Comparing the wall RMS values for θ_3 ($Pr = 0.71$) and θ_5 ($Pr = 2.0$), one can find that they roughly scale as $Pr^{0.6}$ over the present Reynolds number range. It is also noticeable that the maximum RMS values of the scalar fluctuation increase as Pr is increasing. The peak values of the RMS of the scalar fluctuations at $Pr = 2.0$ are about twice as those at $Pr = 0.71$. It is also observed that the peak position moves away from the wall as Pr is decreased. The present DNS results agree well with various results from Kader (1981), Kasagi et al. (1992), and Kawamura et al. (1998) for both the mean profile and the RMS of the scalar fluctuation in the near-wall region.

The previous study by Kawamura et al. (1998) reported that in the vicinity of the wall for isoscalar boundary condition, $\langle \theta \rangle^+$ and

Please cite this article in press as: Li, Q., et al. DNS of a spatially developing turbulent boundary layer with passive scalar transport. Int. J. Heat Fluid Flow (2009), doi:10.1016/j.ijheatfluidflow.2009.06.007

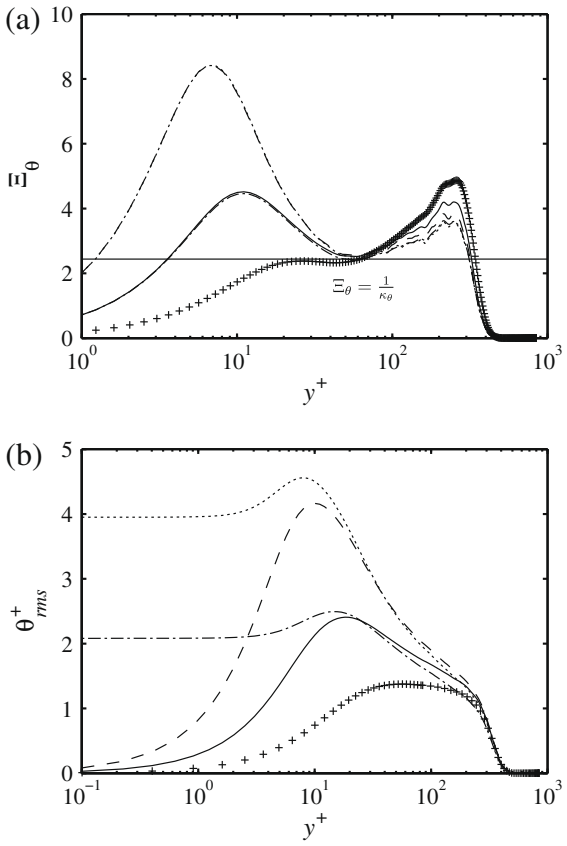

Fig. 8. Profiles of the diagnostic function Ξ_θ with $\kappa_\theta = 0.41$ and scalar variance θ^+_{rms} at $Re_\theta = 830$. + θ_1, — θ_2, -·- θ_3, - - - θ_4, ... θ_5. Isoscalar wall: θ_1, θ_2 and θ_4. Isoflux wall: θ_3 and θ_5. (a) Ξ_θ, (b) θ^+_{rms}.

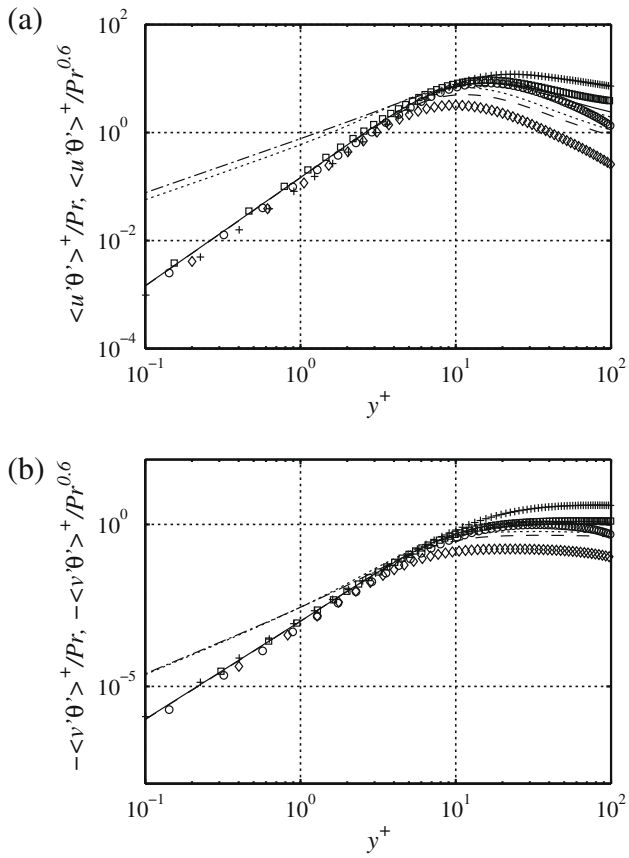

Fig. 9. Profiles of the scalar fluxes $\langle u'\theta'\rangle$ and $-\langle v'\theta'\rangle$ at $Re_\theta = 830$. + θ_1, — θ_2, -·- θ_3, - - - θ_4, ... θ_5. Isoscalar wall: θ_1, $Pr = 0.2$, θ_2, $Pr = 0.71$ and θ_4, $Pr = 2.0$. Isoflux wall: θ_3, $Pr = 0.71$ and θ_5, $Pr = 2.0$. ○ (Kasagi et al., 1992) at $Re_\tau = 150$, $Pr = 0.71$, □ (Abe et al., 2004) at $Re_\tau = 1020$, $Pr = 0.71$, ◇ (Kawamura et al., 1998) at $Re_\tau = 180$, $Pr = 5.0$. (a) $\langle u'\theta'\rangle^+$, (b) $-\langle v'\theta'\rangle^+$.

θ^+_{rms} are proportional to Pry^+ while $\langle u'\theta'\rangle^+$ and $-\langle v'\theta'\rangle^+$ vary as Pry^{+2} and Pry^{+3}, respectively, except for low Pr. This is also true for the present DNS (see Fig. 9) and for the turbulent pipe-flow simulation by Redjem-Saad et al. (2007). For scalars with isoflux boundary condition, using the above exponent for the wall fluctuations, θ^+_{rms} is found proportional to $Pr^{0.6}y^+$ in the vicinity of the wall while the scaling for the mean scalar profile remains the same as for the isoscalar case. For the streamwise and wall-normal scalar fluxes, Kong et al. (2000) concluded that $\langle u'\theta'\rangle^+$ and $-\langle v'\theta'\rangle^+$ are proportional to y^+ and y^{+2}, respectively, based on near-wall asymptotic expansion of u', v' and θ'. Since only one scalar with isoflux wall was computed in their simulation, the relation with Pr is not clear. Based on the present data, $\langle u'\theta'\rangle^+$ and $-\langle v'\theta'\rangle^+$ with isoflux boundary condition vary as $Pr^{0.6}y^+$ and $Pr^{0.6}y^{+2}$, respectively.

An important parameter in scalar transfer is the turbulent Prandtl number Pr_t which is defined as the ratio of the turbulent eddy viscosity ν_t to the eddy diffusivity α_t. ν_t and α_t are defined by

$$\nu_t = -\frac{\langle u'v'\rangle}{\frac{\partial\langle u\rangle}{\partial y}} \tag{17}$$

and

$$\alpha_t = -\frac{\langle v'\theta'\rangle}{\frac{\partial\langle\theta\rangle}{\partial y}}, \tag{18}$$

respectively. The turbulent Prandtl number (see Fig. 10) is often assumed to be a constant value which is independent of the wall-normal distance and the molecular Prandtl number. However, the dependence on the wall-normal position and Pr has long been a subject of many investigations, e.g. Antonia and Kim (1991). For the present DNS, Pr_t for the scalars θ_2 and θ_4 (isoscalar boundary condition) approach approximately a constant value of about 1.1 at the wall independent of the molecular Prandtl number. Both reach their maxima at around $y^+ \approx 45$. Similar values are also reported by previous studies, e.g. Kong et al. (2000) for turbulent boundary-layer flow and Antonia and Kim (1991) for fully developed turbulent channel flow. However, the profile pertaining to the scalar θ_1 with $Pr = 0.2$ is different from the others throughout the boundary layer. The value of Pr_t at the wall for θ_1 is about 0.9 and increases from the wall to the peak value of 1.2 at $y^+ \approx 45$. Bell and Ferziger (1993) obtained a similar peak value for $Pr = 0.1$, but their peak position occurs slightly closer to the wall. In addition, similar to the observation by Bell and Ferziger (1993), the peak values of Pr_t for all the Prandtl numbers are slightly lower than those reported by Kim and Moin (1989) in channel flow. However, Kawamura et al. (1998) found even lower peak values of $Pr = 0.71$ at $Re_\tau = 180$. In the wake region all the Pr_t start increasing again and reach a second peak near the boundary-layer edge. This second peak is due to the intermittency in the wake region of the boundary layer. Comparing with the data from Bell and Ferziger (1993), they only observed the second peak for $Pr = 0.1$, but not for the other Prandtl numbers. Outside the boundary layer, in all cases, Pr_t decreases again.

To analyse the near-wall asymptotic behaviour of the turbulent Prandtl number, one can expand the velocity and scalar distributions in Taylor series as discussed previously. Then the turbulent Prandtl number for the isoscalar wall is found to be constant near the wall while for the isoflux wall it has a linear behaviour with $Pr^{0.4}y^+$. These limiting behaviours are shown in Fig. 10b.

Please cite this article in press as: Li, Q., et al. DNS of a spatially developing turbulent boundary layer with passive scalar transport. Int. J. Heat Fluid Flow (2009), doi:10.1016/j.ijheatfluidflow.2009.06.007

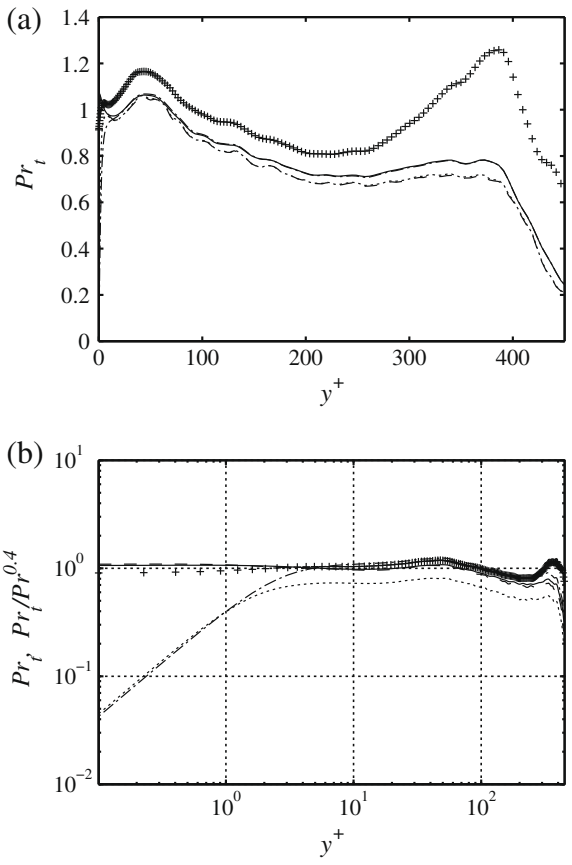

Fig. 10. The wall-normal distribution of the turbulent Prandtl number Pr_t at $Re_\theta = 830$. + θ_1, — θ_2, -·- θ_3, - - - θ_4, ... θ_5. The boundary-layer thickness are ranging from $y^+ = 320$ to $y^+ = 365$ for different scalars.

3.4. Budget equations

From the DNS, the full budgets of the Reynolds-stress and scalar-flux equations are obtained. The transport equations for Reynolds-stresses can be written as

$$\frac{\partial\langle u_i' u_j'\rangle}{\partial t} + C_{ij} = \mathscr{P}_{ij} + \Pi_{ij} + G_{ij} + T_{ij} + D_{ij} - \varepsilon_{ij}, \tag{19}$$

where the interpretations of the different terms can be found e.g. in Pope (2000).

Similarly, the transport equations for the scalar fluxes are given by

$$\frac{\partial\langle u_i'\theta'\rangle}{\partial t} + C_{\theta i} = \mathscr{P}_{\theta i} + \Pi_{\theta i} + G_{\theta i} + T_{\theta i} + \mathscr{D}_{\theta i} - \varepsilon_{\theta i}. \tag{20}$$

The different terms in the Eq. (20) are commonly expanded as

$$C_{\theta i} \equiv \langle u_l\rangle \frac{\partial\langle u_i'\theta'\rangle}{\partial x_l},$$

$$\mathscr{P}_{\theta i} \equiv -\langle u_l'\theta'\rangle \frac{\partial\langle u_i\rangle}{\partial x_l} - \langle u_i' u_l'\rangle \frac{\partial\langle\theta\rangle}{\partial x_l},$$

$$\Pi_{\theta i} \equiv \left\langle p' \frac{\partial\theta'}{\partial x_i}\right\rangle,$$

$$G_{\theta i} \equiv -\frac{\partial\langle p'\theta'\rangle}{\partial x_i},$$

$$T_{\theta i} \equiv -\frac{\partial\langle u_i' u_l'\theta'\rangle}{\partial x_l},$$

$$\mathscr{D}_{\theta i} \equiv \frac{\partial}{\partial x_l}\left(\frac{1}{Pe}\left\langle u_i'\frac{\partial\theta'}{\partial x_l}\right\rangle + \frac{1}{Re_{\delta_0^*}}\left\langle \theta'\frac{\partial u_i'}{\partial x_l}\right\rangle\right),$$

$$\varepsilon_{\theta i} \equiv \left(\frac{1}{Re_{\delta_0^*}} + \frac{1}{Pe}\right)\left\langle \frac{\partial u_i'}{\partial x_l}\frac{\partial\theta'}{\partial x_l}\right\rangle,$$

where $C_{\theta i}$ is denoted as the mean convection, $\mathscr{P}_{\theta i}$ is the production term due to both the mean gradients of velocity and scalar. $\Pi_{\theta i}$ is the pressure scalar-gradient correlation term representing the inter-component redistribution of the turbulent energy between scalar-flux terms. $G_{\theta i}$ is the divergence of the pressure-scalar correlation term which represents spatial redistribution of the energy among different scalar-flux components due to inhomogeneities in the flow field. $\Pi_{\theta i} + G_{\theta i}$ is the scalar pressure-gradient correlation term also denoted as the pressure scrambling term. $T_{\theta i}$ is the turbulent diffusion, which is the divergence of the triple correlation tensor, acting as a spatial redistribution term. $\mathscr{D}_{\theta i}$ is the molecular diffusion term and $\varepsilon_{\theta i}$ the dissipation term.

All the terms in the budget equations are explicitly evaluated including the pressure terms. Two scalings are used: First, a scaling in wall units (inner scaling), i.e. non-dimensionalised by $\frac{u_\tau^4}{\nu}$ for the Reynolds-stress budgets and $\frac{u_\tau^2\theta_\tau}{\nu}$ for the scalar-flux budgets where θ_τ is the friction scalar and defined by $\frac{q_w}{\rho c_p u_\tau}$. Secondly, an outer scaling is used, i.e. quantities are non-dimensionalised by $\frac{U_\infty^3}{\delta^*}$ for the Reynolds-stress budgets and $\frac{U_\infty^2(\theta_\infty-\theta_w)}{\delta_\theta^{99}}$ for the scalar-flux budgets where δ^* is the local displacement thickness and δ_θ^{99} the 99% local scalar boundary-layer thickness. The residual for all the budgets is at most $\mathscr{O}(10^{-3})$ in viscous scaling.

All the Reynolds-stress budgets compare very well with previous studies in both inner and outer scalings, e.g. see Spalart (1988) and Komminaho and Skote (2002). Therefore, these budgets are not discussed further in the interest of space.

In Fig. 11, the budget for the streamwise scalar flux of θ_4 ($Pr = 2.0$) is shown. All the terms are normalised such that the sum of the square of all terms is unity. One can clearly see that the mean convection term, which is negligible near the wall, becomes a major balancing term near the boundary-layer edge, together with the pressure-diffusion and the turbulent diffusion terms. The latter is noticeable in the near-wall region and near the boundary-layer edge, similar as for the Reynolds-stresses. For the case of $\theta_2 (Pr = 0.71)$, the budget for the wall-normal scalar flux $\langle v'\theta'\rangle$ at $Re_\theta = 830$ compares well with the data from Hattori et al. (2007) at a higher Reynolds number $Re_\theta = 1000$.

To further investigate the Pr effects, the budgets of the streamwise and wall-normal scalar fluxes are scaled such that all the dominant terms collapse for both inner and outer scalings. For

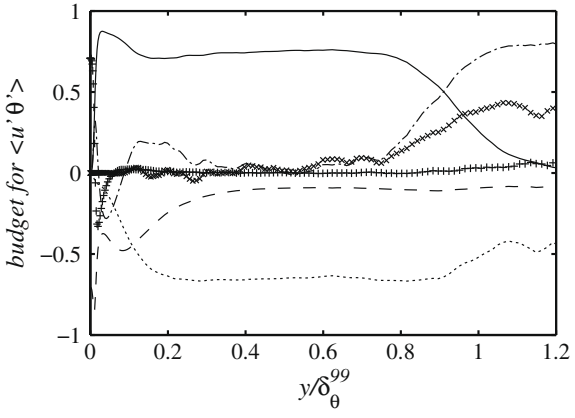

Fig. 11. Budgets of normalised streamwise scalar flux in outer scaling at $Re_\theta = 830$ pertaining to θ_4 with $Pr = 2.0$. — Production, - - - dissipation, —·— turbulent diffusion, ... scalar pressure-diffusion, + molecular diffusion, × mean convection.

Please cite this article in press as: Li, Q., et al. DNS of a spatially developing turbulent boundary layer with passive scalar transport. Int. J. Heat Fluid Flow (2009), doi:10.1016/j.ijheatfluidflow.2009.06.007

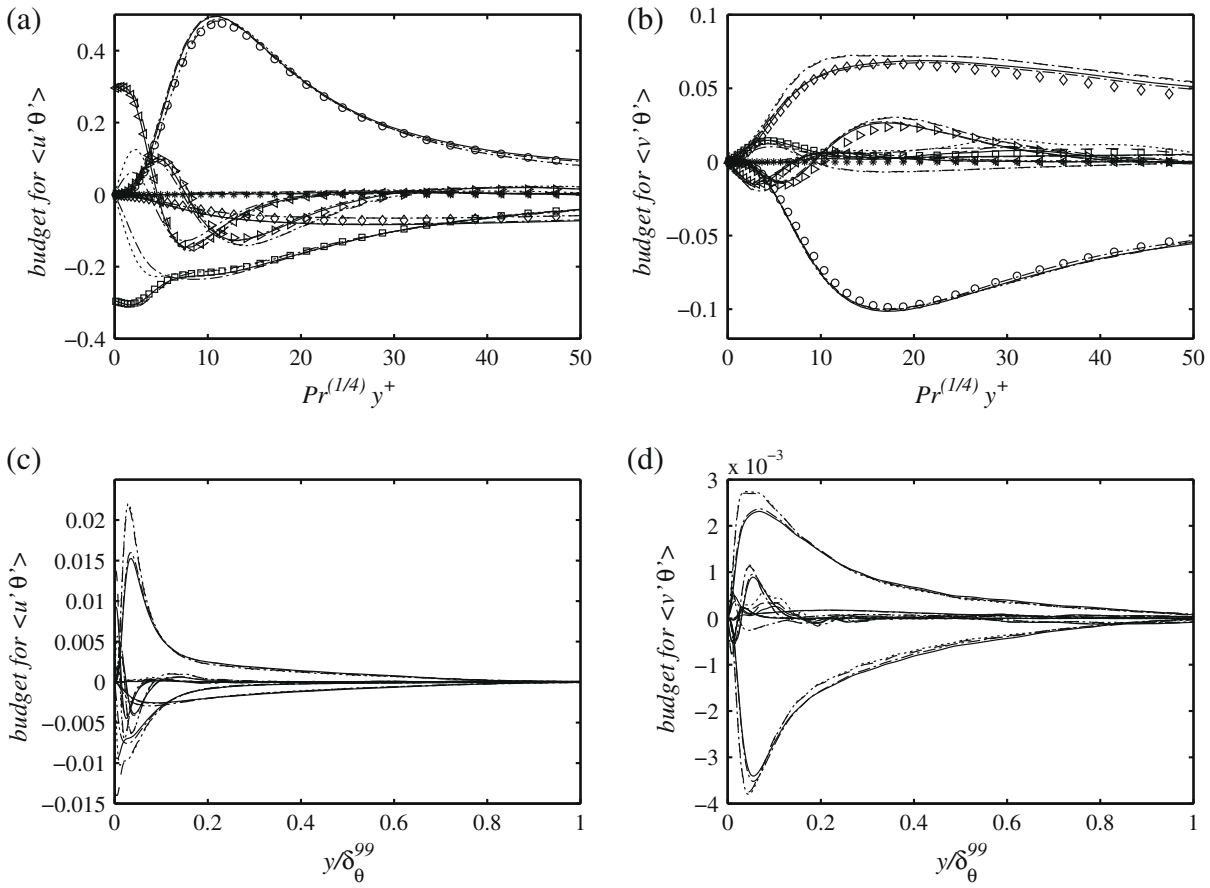

Fig. 12. Prandtl-number dependent scaled budgets of the streamwise and wall-normal scalar fluxes at $Re_\theta = 830$. — θ_2, -·- θ_3, - - - θ_4, ... θ_5, ○ production, □ dissipation, ◇ scalar pressure-diffusion, ◁ molecular diffusion, ▷ turbulent diffusion, ∗ mean convection. Symbols are from Kawamura et al. (1999) at $Re_\tau = 395$ with $Pr = 0.71$. (a) Budget for $\langle u'\theta'\rangle$ in inner scaling. (b) Budget for $\langle v'\theta'\rangle$ in inner scaling. (c) Budget for $\langle u'\theta'\rangle$ in outer scaling. (d) Budget for $\langle v'\theta'\rangle$ in outer scaling.

the budgets in inner scaling as shown in Fig. 12a and b, the streamwise budget $\langle u'\theta'\rangle$ normalised by $Pr^{\frac{1}{2}}$ and the wall-normal budget $\langle v'\theta'\rangle$ normalised by $Pr^{\frac{1}{4}}$ are found to scale with $Pr^{\frac{1}{4}}y^+$. The channel data from Kawamura et al. (1999) with $Pr = 0.71$ at $Re_\tau = 395$ is also included, and very good agreement can be seen for both the streamwise and wall-normal scalar fluxes. For the streamwise scalar fluxes of θ_3 and θ_5, due to the different boundary conditions the agreement with the channel data is only good except in the close vicinity of the wall. The production and dissipation terms are dominant and the molecular diffusion term is only noticeable in the near-wall region. The scalar pressure-gradient correlation term always lies on the loss side and becomes comparable with the dissipation term at $y^+ \approx 40$. Further away from the wall, the scalar pressure-gradient correlation term becomes larger than the dissipation term (see Fig. 11). For the wall-normal scalar flux (see Fig. 12b), a larger but still insignificant difference is observed. The wall boundary condition seems to only influence the dissipation and turbulent diffusion terms and it is less effective in the wall-normal scalar fluxes compared to the streamwise scalar fluxes. The production term is negative for the wall-normal scalar flux. Due to the isotropy in the dissipation scale, the dissipation is negligible for fluids with $Pr \geqslant 0.7$ (Kawamura et al., 1998). This is also true for the present DNS except in the close vicinity of the wall. Thus, the production is balanced mainly by the scalar pressure-gradient correlation term. According to Kawamura et al. (1998), in a low Prandtl-number fluid, the dissipation is dominant because it takes place in eddies of a larger scale. They reported that the scalar pressure-gradient term is dominant for $Pr = 0.4$ and 5.0 while the dissipation term is overwhelming for $Pr = 0.05$. They also reported that the scalar pressure-gradient and the dissipation terms become comparable at $Pr = 0.2$ which is however not true for the present DNS (not shown here).

For the outer scaling as shown in Fig. 12c and d, the budgets are normalised empirically by $Pr^{-\frac{1}{3}}$ to collapse all the curves. The budgets belonging to the scalar with $Pr = 0.2$ are excluded due to low Pr effects. The present scalings are based on the range of Pr of the simulation, therefore further investigations are needed to confirm the validity of the results. In addition, except for the low Pr case, all the budgets of the scalar fluxes $\langle u'\theta'\rangle$ and $\langle v'\theta'\rangle$ look very much like those of the Reynolds-stresses $\langle u'u'\rangle$ and $\langle u'v'\rangle$, respectively. Further discussions concerning low Pr effects can be found in Kasagi and Ohtsubo (1993).

3.5. Higher-order statistics

For a normally distributed random variable, the respective skewness and flatness factors are 0 and 3, respectively. In the near-wall region, the behaviours of the skewness and flatness factors for the velocity and pressure components are similar to those in the channel-flow simulation by Kim et al. (1987). The wall values of the skewness and flatness factors for the pressure fluctuation are −0.04 and 4.9 which are comparable to the results −0.1 and 5.0 obtained by Kim (1989).

The skewness and flatness factors for the scalars are shown in Fig. 13. The profiles of θ_2 and θ_4 compare well with the data by Tohdoh et al. (2008). The skewness factors for the isoflux wall are closer to zero in the vicinity of the wall which implies more symmetric fluctuations than those of the isoscalar wall (Kong

Please cite this article in press as: Li, Q., et al. DNS of a spatially developing turbulent boundary layer with passive scalar transport. Int. J. Heat Fluid Flow (2009), doi:10.1016/j.ijheatfluidflow.2009.06.007

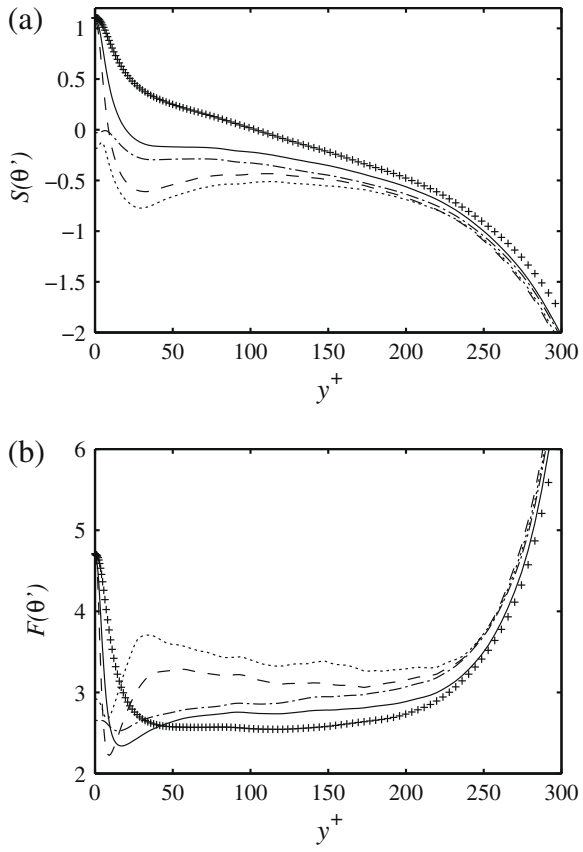

Fig. 13. Skewness and flatness-factor distributions of the scalars at $Re_\theta = 830$. + θ_1, — θ_2, — · — θ_3, - - - θ_4, ... θ_5. (a) Skewness factor $S(\theta')$. (b) Flatness factor $F(\theta')$. The scalar boundary-layer thicknesses at $Re_\theta = 830$ are ranging from $y^+ \approx 320$ to 365.

et al., 2000). Within the conductive sub-layer, $S(\theta')$ with isoscalar wall are positive which is consistent with the positive $S(u')$ (Antonia and Danh, 1977). Redjem-Saad et al. (2007) reported that in a turbulent pipe simulation $F(\theta') = 7$ at the wall for $Pr = 0.71$ which is higher than the present DNS results, which might be due to the surface curvature in the pipe. In addition, $F(\theta')$ reaches its first minimum at about the wall-normal position where the corresponding RMS of the scalar fluctuations are maximum. A similar behaviour can be observed for the streamwise velocity (Durst et al., 1987). An interesting observation is that the effects of the different boundary conditions seem to influence not only the near-wall region; a clear difference can be observed up to $y^+ \approx 150$. On the other hand, the wall values of the higher-order terms for isoscalar boundary condition, i.e. about 1.0 for the skewness and 4.5 for the flatness, appear to be Prandtl-number independent. In the outer region, the skewness and flatness factors increase rapidly which indicates the intermittent region similarly as for the velocity and pressure components. The maximum peak values of $S(\theta')$ and $F(\theta')$ are however much higher than $S(u')$ and $F(u')$ which is also observed in experiments by Antonia and Danh (1977).

3.6. Probability density functions

A different perspective on the characteristics of the fluctuations of one or more variables is provided by analysing the probability density functions (PDF). The PDF distributions of the velocity and pressure fluctuations at various wall-normal positions, ranging from $y^+ \approx 5$ in the viscous sub-layer to $y^+ \approx 500$ in the free-stream (the boundary-layer thickness is about $y^+ = 315$ at $Re_\theta = 830$), are obtained from the simulation as well as the corresponding distributions of the different scalar fluctuations.

The general shape of $P(u')$ agrees well with the experiment study by Durst et al. (1987). For the PDF of the wall-normal velocity fluctuation, Nagano and Tagawa (1988) reported that the distributions are close to the Gaussian distribution in the near-wall region and depart from the Gaussian distribution far away from the wall. However, the present DNS shows more pointy distributions very close to the wall due to the large $F(v')$ values, a behaviour which has been reported virtually for all simulations of wall-bounded turbulence. The PDF of the pressure fluctuation (not shown here) is negatively skewed throughout the boundary layer until the free-stream and the wall-pressure distribution compares well with the data from Kim (1989).

The PDF of the scalar fluctuations of the isoscalar boundary condition are similar to the distributions of the streamwise velocity which reflects the overall similarity between the streamwise velocity u and scalar θ (Antonia et al., 1988). The PDF distribution of $\theta_4(Pr = 2.0)$ is shown in Fig. 14 at different wall-normal positions. A Gaussian distribution with zero mean and matching variance is also included as a reference. All the fluctuations are normalised by the corresponding RMS values and the probability density functions are normalised to unit area. The PDF for the other scalars with isoscalar boundary condition have a similar shape. In particular, a long positive tail at $y^+ \approx 5$ also exists as for streamwise velocity u. This tail is caused by the sweep-type motion of the low momentum fluids and low concentration of scalars (Nagano and Tagawa, 1988). The positive tail shortens with increasing Pr and also with increasing wall-normal distance as shown in Fig. 14. As the Pr or the wall-normal distance is increased, the negative tail extends longer. For the scalars with isoflux boundary condition (not shown here), the PDF distributions are closer to the Gaussian distribution in the near-wall region. Far away from the wall ($y^+ > 50$), there is no noticeable difference between the distributions with the different boundary conditions. At $y^+ \approx 300$, all the PDF of the scalar fluctuations are extremely negatively skewed which indicates the existence of the intermittent region. In the free-stream, as expected, the profiles are again close to the Gaussian distribution with extremely small variance.

The high correlation between streamwise velocity and the scalar is also illustrated by the joint probability density function (JPDF). The results of θ_2' at $y^+ \approx 5$ are consistent with the previous results from a channel DNS simulation by Kim and Moin (1989). JPDF of (u', θ') of $Pr = 2.0$ at $y^+ \approx 5$ and $Re_\theta = 830$ are shown in Fig. 15. A less correlated relation between the streamwise velocity and the scalars with isoflux boundary condition is observed, indicating the influence of the different boundary conditions for u and θ for these cases.

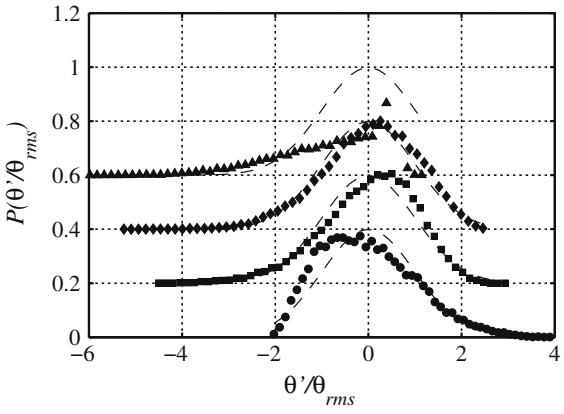

Fig. 14. PDF of θ_4' with $Pr = 2.0$ and isoscalar wall at $Re_\theta = 830$ with boundary-layer edge at $y^+ = 320$. • $y^+ \approx 5$, ■ $y^+ \approx 50$, ♦ $y^+ \approx 100$, ▲ $y^+ \approx 300$, - - - Gaussian distribution.

Please cite this article in press as: Li, Q., et al. DNS of a spatially developing turbulent boundary layer with passive scalar transport. Int. J. Heat Fluid Flow (2009), doi:10.1016/j.ijheatfluidflow.2009.06.007

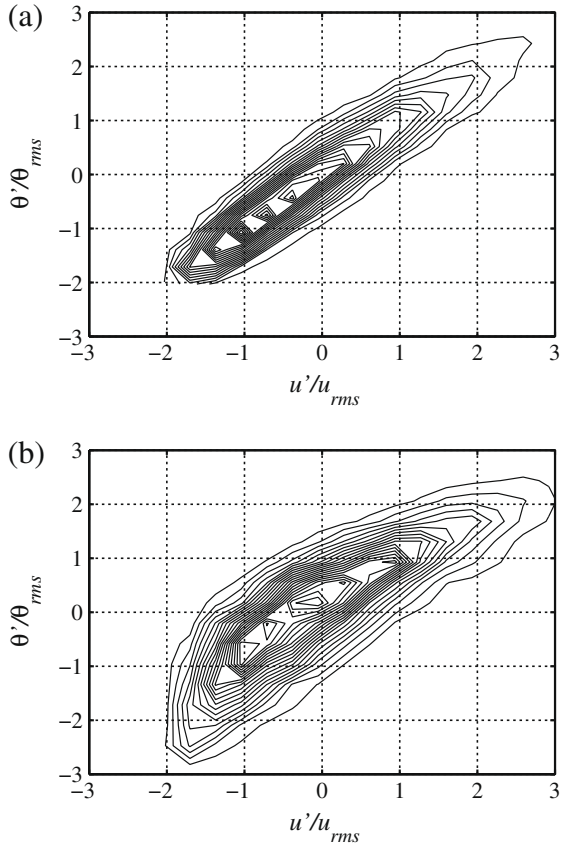

Fig. 15. JPDF of (u', θ') $(Pr = 2.0)$ at $y^+ \approx 5$ with $Re_\theta = 830$. (a) $P(u', \theta'_4)$, (b) $P(u', \theta'_5)$. Contour levels are 0.025:0.025:0.5 for (a) and 0.016:0.016:0.32 for (b).

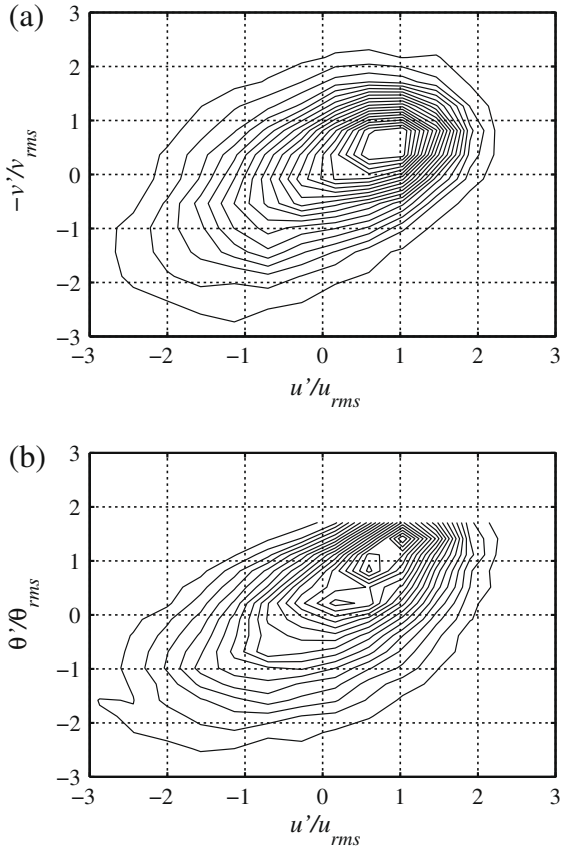

Fig. 16. JPDF of $(u', -v')$ and (u', θ'_2) at $y^+ \approx 200$ with $Re_\theta = 830$. (a) $P(u', -v')$, (b) $P(u', \theta'_2)$. Contour levels are 0.012:0.012:0.24 for (a) and from 0.01:0.01:0.2 for (b).

The JPDF of (u', θ'_2) and $(u', -v')$ at $y^+ \approx 200$ with $Re_\theta = 830$ are shown in Fig. 16. Far away from the wall, all the JPDF distributions show mildly correlated shapes as expected. The scalar boundary condition has almost no effect at this wall-normal position. It is noticeable that not all the contours have their centres located at the origin and the peaks of (u', θ') moves from the third quadrant to the first quadrant as the wall-normal position increases.

Note that in JPDF Fig. 15a and b, one can observe a sharp cutoff for the scalar fluctuation θ'. This is caused by the Dirichlet boundary condition, which bounds the scalar values to be between θ_w and θ_∞. In consequence, the scalar fluctuations have strict lower and upper bounds, depending on the local mean values.

3.7. Spanwise two-point correlation

The spanwise two-point correlations of the velocity components and pressure at $Re_\theta = 830$ at several wall-normal positions from $y^+ \approx 5$ to $y^+ \approx 300$ are obtained. In general the results are consistent with the numerical results by Kim et al. (1987). As also observed by Kim (1989), the spanwise two-point correlation coefficient of the pressure does not have the negative excursion.

The spanwise two-point correlations of the scalars near the wall are similar to those observed by Kim and Moin (1989). On the other hand, the scalars of the isoflux boundary condition seem to be much more affected by the Prandtl number. In general, scalars with isoflux wall have larger mean spanwise spacings than those of the isoscalar wall (Kong et al., 2000). Far from the wall, the boundary conditions do not have an influence on the profiles.

For the mean low-speed streak and scalar streak spacings obtained from twice the first minimum of the spanwise two-point correlations, the results for θ_2 and θ_3 compare well with Kong et al. (2000). As also noted by Kong et al. (2000) that the low-speed streak spacing is similar to that of θ_2 and the differences from the boundary conditions are only observable in the near-wall region. One can also observe that the mean scalar streak spacings are larger for smaller Pr near the wall. Due to the isoflux wall-boundary condition, the scalar spacings first decrease and then increase again as being away from the wall (not shown here). The streamwise evolution of the mean streak spacings at $y^+ \approx 7$ from $Re_\theta = 390$ to $Re_\theta = 830$ is shown in Fig. 17. In general all the steak spacings grow slightly downstream with increasing Reynolds numbers, however, the growth rate levels off towards larger Reynolds numbers. The large growth rate in the low Reynolds number range may be due to a low Reynolds-number effect (Antonia and Kim, 1994). At $Re_\theta = 830$, the streaks have a spacing of about 110 in wall unit which is slightly larger than the usual value of about 100 (Kim et al., 1987). On the other hand, this spacing is in good agreement with recent studies in turbulent boundary layer by Schlatter et al. (in press). These authors also found that the velocity streak spacing continues to grow up to $Re_\theta = 1500$ and then settles at a constant value around 115. The streaks pertaining to scalars with isoflux boundary condition are growing faster than those with isoscalar boundary condition at the same Pr. It is also suggested by the present results that the streak spacing with lower Pr grows faster. It has also been shown by Österlund (1999) and Abe et al. (2001)) that the spanwise two-point correlations of the wall-shear stress τ_w and streamwise velocity fluctuation u' have less prominent negative peaks with increasing Reynolds number, which is confirmed

Please cite this article in press as: Li, Q., et al. DNS of a spatially developing turbulent boundary layer with passive scalar transport. Int. J. Heat Fluid Flow (2009), doi:10.1016/j.ijheatfluidflow.2009.06.007

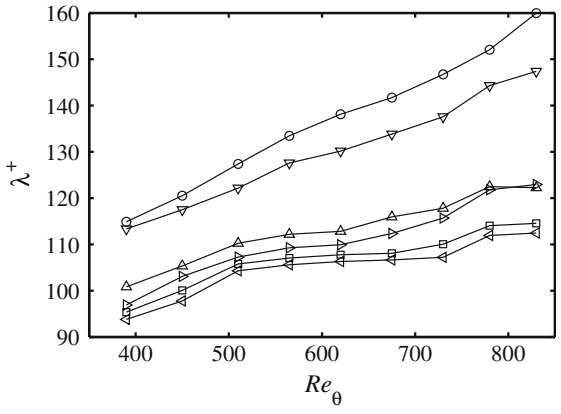

Fig. 17. Streamwise variation of the mean spanwise streaks spacing λ^+ at $y^+ \approx 7$. □ u, ○ θ_1, △ θ_2, ▽ θ_3, ◁ θ_4, ▷ θ_5.

by the present DNS. This effect is due to the dominating large-scale structures which scale with outer units, i.e. the boundary-layer thickness or the channel half width, see also Schlatter et al. (in press). Schlatter et al. (in press) also showed that at least $Re_\theta = 1500$ is needed to clearly observe a second peak indicating the footprint of the large-scale structure in a contour plot of the two-point correlation of the wall-shear stress τ_w versus the Reynolds number. Concerning the scalar two-point correlations, Abe et al. (2004) showed that less prominent negative peaks with increasing Reynolds number only exist for the surface heat flux q_w with $Pr = 0.71$, but not for the case with $Pr = 0.025$ due to a low Prandtl-number effect. However, for the Pr-range considered here, all scalars irrespective of the boundary condition feature a decreasing near-wall (inner) peak.

The spanwise two-point correlations not only contain the information about the spanwise organisation of the near-wall streaks but also the large-scale motions in the outer region of the boundary layer. By showing the premultiplied spanwise spectra $k_z\Phi_{uu}(\lambda_z)$ of the streamwise velocity u, both experiment (e.g. Hutchins and Marusic, 2007) and simulation (e.g. del Álamo and Jiménez, 2003) showed evidence of the large-scale structures existing in the outer layer. For the scalar field, (Abe and Kawamura, 2002) reported the existence of the large-scale structure in the outer layer of the channel for $Re_\tau = 640$ with $Pr = 0.025$ and 0.71, but no detailed discussion was provided. Fig. 18a shows the one-dimensional spanwise spectra $k_z\Phi_{uu}(\lambda_z)$ and $k_z\Phi_{\theta_2\theta_2}(\lambda_z)$ scaled with u_τ^2 and θ_τ^2, respectively, at $Re_\theta = 830$. In general, both spectra are similar in appearance with the inner peak located at $y^+ \approx 15$ (see also Fig. 8b) and $\lambda_z \approx 110$ indicating the near-wall streaks. However, differences can be observed in the outer region ($y^+ > 100$) where the outer peak of θ_2 is weaker than that of u. Fig. 18b shows the spanwise spectra for scalars θ_4 and θ_5 with different boundary conditions but same $Pr = 2.0$. The influence of the different boundary conditions is clearly seen. The spectrum of θ_5 with isoflux boundary condition has a constant value down to the wall whereas the spectrum of θ_4 is decreasing to zero to fulfil the boundary condition. Above $y^+ = 10$, there is no clear difference. Compared to Fig. 18a, it is important to note that the outer peak ($\lambda_z^+ \approx 400$) does not exist for $Pr = 2.0$. Fig. 18c shows Pr effects on the spanwise spectra. With increasing Pr, the spectral peaks move towards the wall and towards smaller spanwise wavelengths λ_z (see also Fig. 17). Note that the inner peak for the case of $Pr = 0.2$ resides at $y^+ \approx 50$ which is also observed in the RMS value of the scalar variance as shown in Fig. 8b. If the spanwise spectrum of θ_1 ($Pr = 0.2$) is scaled by θ_{rms}^2 instead of θ_τ^2, the peak extends towards $y^+ \approx 10$, however the corresponding fluctuations θ_{rms} close to the wall are extremely small.

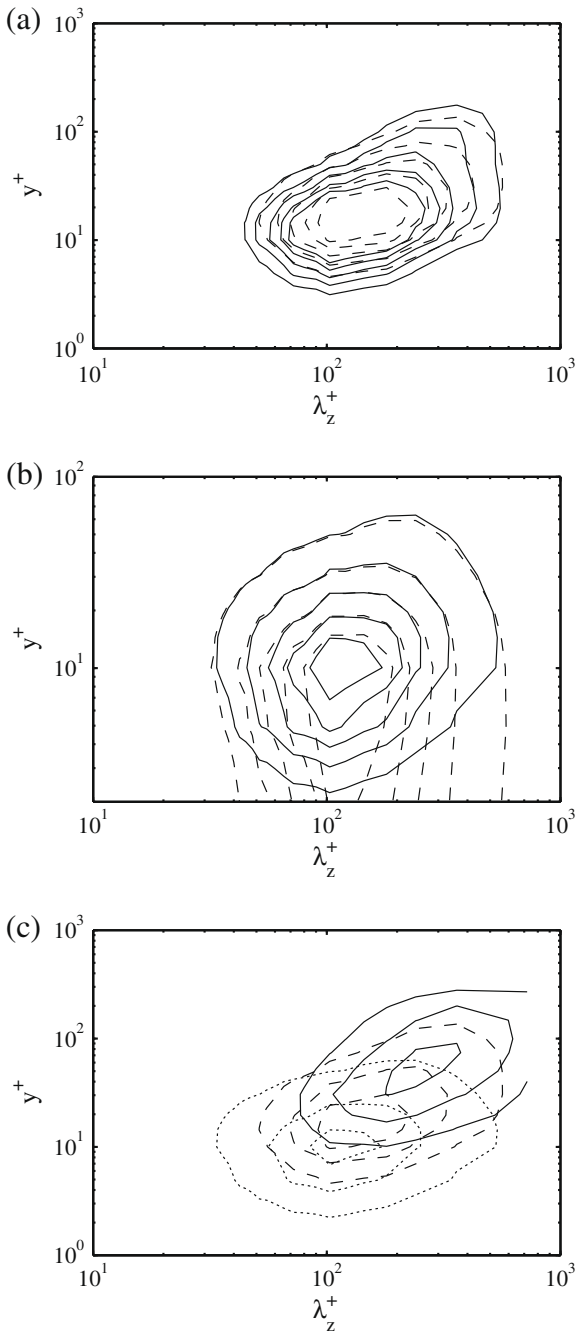

Fig. 18. Premultiplied energy spectra of the streamwise velocity and scalars at $Re_\theta = 830$. (a) — $k_z\Phi_{uu}(\lambda_z)/u_\tau^2$, - - - $k_z\Phi_{\theta_2\theta_2}(\lambda_z)/\theta_\tau^2$, (b) $k_z\Phi_{\theta\theta}(\lambda_z)/\theta_\tau^2$ at $Pr = 2.0$, — isoscalar boundary condition, - - - isoflux boundary condition, (c) $k_z\Phi_{\theta\theta}(\lambda_z)/\theta_\tau^2$ with isoscalar boundary condition, —— $Pr = 0.2$, - - - $Pr = 0.71$, ... $Pr = 2.0$. Contour levels are 1:0.375:2.5 in (a); 2:1.5:8 in (b); and 0.3:0.3:0.9 for $Pr = 0.2$, 1:0.75:2.5 for $Pr = 0.71$ and 2:3:8 for $Pr = 2.0$ in (c).

4. Conclusions

A direct numerical simulation (DNS) of a spatially developing turbulent boundary layer with passive scalars over a flat plate under zero pressure-gradient (ZPG) has been carried out. The Reynolds number based on the inlet displacement thickness $Re_{\delta_0^*}$ is 450, and Prandtl numbers are varying from 0.2 to 2 while two wall-boundary conditions, i.e. isoscalar and isoflux, are employed. The highest Reynolds number obtained is $Re_\theta = 850$ based on the momentum thickness θ. The computed velocity and scalar fields

Please cite this article in press as: Li, Q., et al. DNS of a spatially developing turbulent boundary layer with passive scalar transport. Int. J. Heat Fluid Flow (2009), doi:10.1016/j.ijheatfluidflow.2009.06.007

are compared with existing data from the literature and the agreement is very good in general.

The main conclusions of the present study are summarised as follows:

- The mean scalar profiles are virtually independent of the employed wall-boundary conditions whereas the effects on the scalar variances are obvious in the near-wall region. Further away from the wall, the effects from different wall-boundary conditions are negligible. The skewness and flatness profiles are different up to about 150 in viscous units, i.e. to the middle of the boundary layer for the present simulation parameters.
- The results (mean scalar profiles, Pr_t, JPDF, two-point correlations etc.) for θ_2 with $Pr = 0.71$ and isoscalar boundary condition obtained from the present DNS and those from Kim and Moin (1989) using an internal heat source appear similar in the near-wall region. This implies that these two boundary conditions might not have a significant influence on the low-order statistics in the near-wall region.
- All the terms in the Reynolds-stress and scalar-flux budgets are explicitly evaluated including the pressure terms. Far away from the wall, both the mean convection and the turbulent diffusion term become balancing terms in the scalar-flux budgets, together with the pressure-diffusion term. This is in good agreement to the Reynolds-stress budgets.
- Prandtl-number scalings for the scalar-flux budgets and several other scalar quantities in both inner and outer units are proposed based on the present data, however, further investigations at wider Pr range are needed to validate the results.
- The intermittency in the outer region is identified and quantified via higher-order statistics and PDF distributions.
- The scalar with isoscalar boundary condition is highly correlated with the streamwise velocity component in the near-wall region, however showing the influence of the wall-boundary condition. Near the boundary-layer edge, a mild correlation between these two quantities was observed, especially independent of the boundary condition.
- All the scalar streak spacings grow downstream with increasing Reynolds numbers. The scalar streak spacings pertaining to the isoflux boundary condition and lower Pr grow faster.
- The large-scale structures could be identified with the help of the premultiplied spanwise energy spectra. There certainly exist large-scale structures for the velocity field and scalar with $Pr = 0.71$. For the higher Pr cases, no large-scale structures are identified. The inner spectra peaks move away from the wall and towards larger wavelengths λ_z as Pr decreases.
- Even though the Reynolds number considered in the present study is so far the highest with such a variety of scalars, it is still low compared to the experiments. Therefore, low Reynolds number effects are important and play a role when interpreting the results.

In the future, the large amount of data from the simulation will be further processed and new and existing LES/RANS closures for modelling the scalar fluxes will be developed and critically evaluated against the present database.

The present database will be open to public access through the following link: http://www.mech.kth.se/.

Acknowledgements

Computer time was provided by the Center for Parallel Computers (PDC) at the Royal Institute of Technology (KTH) and the National Supercomputer Center (NSC) at Linköping University in Sweden.

References

Abe, H., Kawamura, H., 2002. A study of turbulence thermal structure in a channel flow through DNS up to $Re_\tau = 640$ with $Pr = 0.025$ and 0.71. In: Castro, I.P., Hancock, P.E., Thomas, T.G. (Eds.), Advances in Turbulence IX. CIMNE, Barcelona, Spain, pp. 399–402.

Abe, H., Kawamura, H., Matsuo, Y., 2001. Direct numerical simulation of a fully developed turbulent channel flow with respect to the Reynolds number dependence. J. Fluids Eng. 123 (2), 382–393.

Abe, H., Kawamura, H., Matsuo, Y., 2004. Surface heat-flux fluctuations in a turbulent channel flow up to $Re_\tau = 1020$ with $Pr = 0.025$ and 0.71. Int. J. Heat Fluid Flow 25 (3), 404–419.

Antonia, R.A., Danh, H.Q., 1977. Structure of temperature fluctuations in a turbulent boundary layer. Phys. Fluids 20 (7), 1050–1057.

Antonia, R.A., Kim, J., 1991. Turbulent Prandtl number in the near-wall region of a turbulent channel flow. Int. J. Heat Mass Transfer 34 (7), 1905–1908.

Antonia, R.A., Kim, J., 1994. Low-Reynolds-number effects on near-wall turbulence. J. Fluid Mech. 276, 61–80.

Antonia, R.A., Krishnamoorthy, L.V., Fulachier, L., 1988. Correlation between the longitudinal velocity fluctuation and temperature fluctuation in the near-wall region of a turbulent boundary layer. Int. J. Heat Mass Transfer 31 (4), 723–730.

Bell, D.M., Ferziger, J.H., 1993. Turbulent boundary layer dns with passive scalars. In: So, R.M.C., Speziale, C.G., Launder, B.E. (Eds.), Near-Wall Turbulent Flows. Elsevier, pp. 327–366.

Bertolotti, F.P., Herbert, T., Spalart, P.R., 1992. Linear and nonlinear stability of the Blasius boundary layer. J. Fluid Mech. 242, 441–474.

Brandt, L., Schlatter, P., Henningson, D.S., 2004. Transition in boundary layers subject to free-stream turbulence. J. Fluid Mech. 517, 167–198.

Chevalier, M., Schlatter, P., Lundbladh, A., Henningson, D.S., 2007. A pseudo-spectral solver for incompressible boundary layer flows. Tech. Rep. TRITA-MEK 2007:07, Royal Institute of Technology, Stockholm.

Corrsin, S., 1952. Heat transfer in isotropic turbulence. J. Appl. Phys. 23 (1), 113–118.

del Álamo, J.C., Jiménez, J., 2003. Spectra of the very large anisotropic scales in turbulent channels. Phys. Fluids 15 (6), L41–L44.

Durst, F., Jovanovic, J., Kanevce, L., 1987. Probability density distribution in turbulent wall boundary-layer flows. In: Durst, F., Launder, B.E., Lumley, J.L., Schmidt, F.W., Whitelaw, J.H. (Eds.), Turbulent Shear Flows 5. Springer-Verlag, Berlin, pp. 197–220.

Hattori, H., Houra, T., Nagano, Y., 2007. Direct numerical simulation of stable and unstable turbulent thermal boundary layers. Int. J. Heat Fluid Flow 28 (6), 1262–1271.

Hetsroni, G., Kowalewski, T.A., Hu, B., Mosyak, A., 2001. Tracking of coherent thermal structures on a heated wall by means of infrared thermography. Exp. Fluids 30 (3), 286–294.

Hishida, M., Nagano, Y., 1979. Structure of turbulent velocity and temperature fluctuations in fully developed pipe flow. ASME J. Heat Transfer 101, 15–22.

Hutchins, N., Marusic, I., 2007. Evidence of very long meandering features in the logarithmic region of turbulent boundary layers. J. Fluid Mech. 579, 1–28.

Kader, B.A., 1981. Temperature and concentration profiles in fully turbulent boundary layers. Int. J. Heat Mass Transfer 24 (9), 1541–1544.

Kasagi, N., Ohtsubo, Y., 1993. Direct numerical simulation of low Prandtl number thermal fluid in a turbulent channel flow. In: Durst, F. (Ed.), Turbulent Shear Flows 8. Springer-Verlag, Berlin, pp. 97–119.

Kasagi, N., Tomita, Y., Kuroda, A., 1992. Direct numerical simulation of passive scalar field in a turbulent channel flow. ASME J. Heat Transfer 114, 598–606.

Kawamura, H., Abe, H., Matsuo, Y., 1999. DNS of turbulent heat transfer in channel flow with respect to reynolds and prandtl number effects. Int. J. Heat Fluid Flow 20 (3), 196–207.

Kawamura, H., Ohsaka, K., Abe, H., Yamamoto, K., 1998. DNS of turbulent heat transfer in channel flow with low to medium-high Prandtl number fluid. Int. J. Heat Fluid Flow 19 (5), 482–491.

Kays, W.M., Crawford, M.E., 1993. Convective Heat and Mass Transfer, third ed. McGraw-Hill, New York, USA.

Kim, J., 1989. On the structure of pressure fluctuations in simulated turbulent channel flow. J. Fluid Mech. 205, 421–451.

Kim, J., Moin, P., 1989. Transport of passive scalars in a turbulent channel flow. In: André, J.-C., Cousteix, J., Durst, F., Launder, B.E., Schmidt, F.W. (Eds.), Turbulent Shear Flows, vol. 6. Springer-Verlag, Berlin, pp. 85–96.

Kim, J., Moin, P., Moser, R., 1987. Turbulence statistics in fully developed channel flow at low Reynolds number. J. Fluid Mech. 177, 133–166.

Komminaho, J., Skote, M., 2002. Reynolds stress budgets in Couette and boundary layer flows. Flow Turbul. Combust. 68 (2), 167–192.

Kong, H., Choi, H., Lee, J.S., 2000. Direct numerical simulation of turbulent thermal boundary layers. Phys. Fluids 12 (10), 2555–2568.

Krishnamoorthy, L.V., Antonia, R.A., 1987. Temperature-dissipation measurements in a turbulent boundary layer. J. Fluid Mech. 176, 265–281.

Li, Q., Schlatter, P., Brandt, L., Henningson, D.S., 2008. Direct numerical simulation of a turbulent boundary layer with passive scalar transport. Direct and Large-Eddy Simulation, vol. VII. Springer-Verlag, Berlin.

Mosyak, A., Pogrebnyak, E., Hetsroni, G., 2001. Effect of constant heat flux boundary condition on wall temperature fluctuations. ASME J. Heat Transfer 123 (2), 213–218.

Nagano, Y., Tagawa, M., 1988. Statistical characteristics of wall turbulence with a passive scalar. J. Fluid Mech. 196, 157–185.

Please cite this article in press as: Li, Q., et al. DNS of a spatially developing turbulent boundary layer with passive scalar transport. Int. J. Heat Fluid Flow (2009), doi:10.1016/j.ijheatfluidflow.2009.06.007

Nagib, H.M., Chauhan, K.A., Monkewitz, P.A., 2007. Approach to an asymptotic state for zero pressure gradient turbulent boundary layers. Phil. Trans. Roy. Soc. A 365, 755–770.

Nordström, J., Nordin, N., Henningson, D.S., 1999. The fringe region technique and the Fourier method used in the direct numerical simulation of spatially evolving viscous flows. SIAM J. Sci. Comp. 20 (4), 1365–1393.

Österlund, J.M., 1999. Experimental Studies of Zero Pressure-gradient Turbulent Boundary Layer Flow. Ph.D. thesis, Royal Institute of Technology, Stockholm, Sweden.

Österlund, J.M., Johansson, A.V., Nagib, H.M., Hites, M.H., 1999. Wall shear stress measurements in high Reynolds number boundary layers from two facilities. AIAA J., 1999–3814.

Perry, A.E., Hoffmann, P.H., 1976. An experimental study of turbulent convective heat transfer from a flat plate. J. Fluid Mech. 77, 355–368.

Pope, S.B., 2000. Turbulent Flows. Cambridge University Press, Cambridge, UK.

Purtell, L.P., Klebanoff, P.S., Buckley, F.T., 1981. Turbulent boundary layer at low Reynolds number. Phys. Fluids 24 (5), 802–811.

Redjem-Saad, L., Ould-Rouiss, M., Lauriat, G., 2007. Direct numerical simulation of turbulent heat transfer in pipe flows: effect of Prandtl number. Int. J. Heat Fluid Flow 28 (5), 847–861.

Roach, P.E., Brierley, D.H., 1992. The influence of a turbulent freestream on zero pressure gradient transitional boundary layer development part I: Test cases, T3A and T3B. In: Numerical Simulation of Unsteady Flows and Transition to Turbulence, ERCOFTAC. Cambridge University Press, Cambridge, U.K, pp. 319–347.

Rogers, M., Moin, P., Reynolds, W., 1986. The structure and modeling of the hydrodynamic and passive scalar fields in homogeneous turbulent shear flow. Tech. Rep. TF-25, Stanford University, USA.

Schlatter, P., Örlü, R., Li, Q., Brethouwer, G., Fransson, J.H. M., Johansson, A.V., Alfredsson, P.H., Henningson, D.S., 2009. Turbulent boundary layers up to $Re_{theta} = 2500$ studied through simulation and experiment. Phys. Fluids 21 (5), 051702.

Spalart, P.R., 1988. Direct simulation of a turbulent boundary layer up to $Re_{\theta} = 1410$. J. Fluid Mech. 187, 61–98.

Subramanian, C.S., Antonia, R.A., 1981. Effect of Reynolds number on a slightly heated turbulent boundary layer. Int. J. Heat Mass Transfer 24 (11), 1833–1846.

Tiselj, I., Bergant, R., Mavko, B., Bajsić, I., Hetsroni, G., 2001. DNS of turbulent heat transfer in channel flow with heat conduction in the solid wall. ASME J. Heat Transfer 123, 849–857.

Tohdoh, K., Iwamoto, K., Kawamura, H., 2008. Direct numerical simulation of passive scalar transport in a turbulent boundary layer. In: Proceedings of the 7th International ERCOFTAC Symposium on Engineering Turbulence Modelling and Measurements, Limassol, Cyprus, 2008. pp. 169–174.

Warhaft, Z., Lumley, J.L., 1978. An experimental study of the decay of temperature fluctuations in grid-generated turbulence. J. Fluid Mech. 88, 659–685.

Wikström, P., 1998. Measurements, Direct Numerical Simulation and Modeling of Passive Scalar Transport in Turbulent Flows. Ph.D. thesis, Royal Institute of Technology, Stockholm, Sweden.

Please cite this article in press as: Li, Q., et al. DNS of a spatially developing turbulent boundary layer with passive scalar transport. Int. J. Heat Fluid Flow (2009), doi:10.1016/j.ijheatfluidflow.2009.06.007